ARTICLES
PUBLISHED ONLINE: 12 DECEMBER 2010 | DOI: 10.1038/NCHEM.929
nature chemistry

Control and imaging of $O(^1D_2)$ precession

Shiou-Min Wu[1], Dragana Č. Radenovic[1], Wim J. van der Zande[1], Gerrit C. Groenenboom[1], David H. Parker[1]*, Claire Vallance[2]* and Richard N. Zare[3]*

Larmor precession of a quantum mechanical angular momentum vector about an applied magnetic field forms the basis for a range of magnetic resonance techniques, including nuclear magnetic resonance spectroscopy and magnetic resonance imaging. We have used a polarized laser pump–probe scheme with velocity-map imaging detection to visualize, for the first time, the precessional motion of a quantum mechanical angular momentum vector. Photodissociation of O_2 at 157 nm provides a clean source of fast-moving $O(^1D_2)$ atoms, with their electronic angular momentum vector strongly aligned perpendicular to the recoil direction. In the presence of an external magnetic field, the distribution of atomic angular momenta precesses about the field direction, and polarization-sensitive images of the atomic scattering distribution recorded as a function of field strength yield 'time-lapse-photography' style movies of the precessional motion. We present movies recorded in various experimental geometries, and discuss potential consequences and applications in atmospheric chemistry and reaction dynamics.

Nuclear magnetic resonance spectroscopy, electron spin resonance spectroscopy and magnetic resonance imaging have revolutionized medicine and the chemical sciences. They have provided detailed structure determination and quantification capabilities for chemical species in liquid or solid phases, and a battery of state-of-the-art medical imaging techniques. All three techniques are based on the quantum-mechanical phenomenon of Larmor precession.

Every quantum-mechanical angular momentum vector, including nuclear spin, '**I**', electronic spin, '**S**' and electronic orbital angular momentum, '**L**', has an associated magnetic moment. For a spin-zero system such as the $O(^1D_2)$ atom considered in this paper, the magnetic moment $\boldsymbol{\mu}$ is related to the angular momentum **J** by

$$\boldsymbol{\mu} = -\frac{e}{2m_e}\mathbf{J} \tag{1}$$

where e and m_e are the electronic charge and mass, respectively. When an external magnetic field **B** is applied to the system, the magnetic moment experiences a torque, $\boldsymbol{\tau} = \boldsymbol{\mu} \times \mathbf{B}$, perpendicular to the magnetic moment (and therefore perpendicular to the angular momentum **J**), which causes the magnetic moment to precess about the field direction. This motion is known as Larmor precession, and occurs at the Larmor precession frequency[1]

$$\nu_L = \frac{\mu_B B}{h} \tag{2}$$

where $\mu_B = e\hbar/2m_e$ is the electronic Bohr magneton.

In this contribution, we use velocity-map imaging (VMI) to visualize Larmor precession of an ensemble of atomic orbital angular momentum vectors in the presence of an external magnetic field. VMI is a technique developed in the field of chemical reaction dynamics for imaging atomic and molecular scattering distributions arising from photoinitiated unimolecular and bimolecular reactions. Of particular relevance to this work, the technique may be used to measure the spatial distribution of an atomic or molecular angular momentum vector.

To observe Larmor precession, we must first create a strongly aligned distribution of atomic angular momentum vectors (this is analogous to preparing an 'overall magnetization' vector in NMR techniques). As explained below, $O(^1D_2)$ atoms formed in the 157 nm photolysis of molecular oxygen provide a uniquely clean and simple system in which to explore Larmor precession.

The first excited $O(^1D_2)$ state of atomic oxygen lies 1.967 eV above the $O(^3P_2)$ ground state. This high energy, together with its open-shell character, makes $O(^1D_2)$ highly reactive in collisions with other atomic or molecular species. In the absence of collisions, however, $O(^1D)$ is metastable[2] with a lifetime of ~110 ns, a consequence of the fact that emission of a photon to return the atom to the ground state is spin forbidden. This long lifetime greatly facilitates the study of processes involving $O(^1D)$.

As $O(^1D_2)$ is a singlet state, the spin quantum number is zero, and the atomic angular momentum **J** is determined simply by the electronic orbital angular momentum, **L**, which for $O(^1D_2)$ has a quantum number $L = 2$. The description of angular momentum polarization in this system is particularly straightforward, as the M_J and M_L quantum numbers, describing the projections of the total and orbital electronic angular momenta onto a fixed axis, are equivalent. The situation is simplified even further by the fact that the overwhelmingly predominant ^{16}O isotope of oxygen has no nuclear spin, so there is no hyperfine depolarization of the nascent angular momentum distribution caused by coupling of the electronic angular momentum to the nuclear spin. In combination, these factors make $O(^1D)$ a very promising candidate for the study of chemical reactivity as a function of atomic polarization[3,4], an idea that is explored further later in this paper.

Because the electronic angular momentum of an atom or molecule is determined by the distribution of unpaired electron density, which is often highly anisotropic during the process of bond cleavage, many chemical processes yield products in which the electronic angular momentum is strongly polarized. Dissociation of O_2 through the $B^3\Sigma_u^-$ state provides a good

[1]Radboud University Nijmegen, Institute for Molecules and Materials (IMM), Heyendaalseweg 135, 6525 AJ, Nijmegen, The Netherlands, [2]Department of Chemistry, University of Oxford, Chemistry Research Laboratory, 12 Mansfield Road, Oxford OX1 3TA, UK, [3]Department of Chemistry, Stanford University, 333 Campus Drive, Stanford, California 94305-5080, USA. *e-mail: parker@science.ru.nl; claire.vallance@chem.ox.ac.uk; zare@stanford.edu

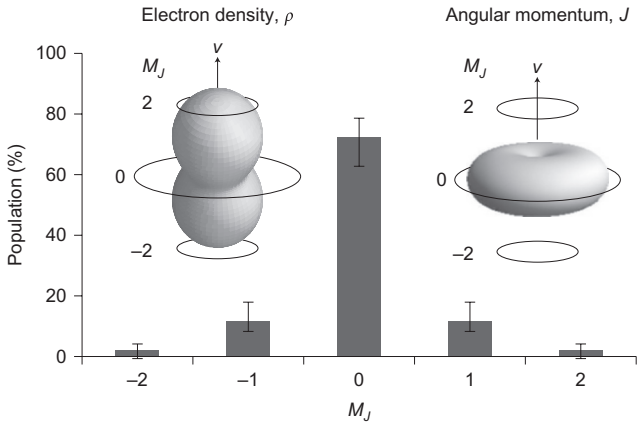

Figure 1 | The O($^1D_2$) M_J state population distribution following photodissociation of O_2 at 157 nm. For axial recoil, M_J is the quantum number describing the projection of the O-atom orbital angular momentum J onto the recoil velocity direction **v**. The corresponding electron density and angular momentum distribution are also shown. (Data from ref. 7.). The error bars are one standard deviation of the population values from several data sets consisting of numerous images recorded in different experimental geometries using two different probe transitions.

example, and we will consider its dissociation dynamics in some detail. Excitation from the $X^3\Sigma_g^-$ ground state to the $B^3\Sigma_u^-$ state is the first allowed optical transition in O_2, occurring at wavelengths below 175 nm. The transition gives rise to the well-known Schumann–Runge bands and continuum in the absorption spectrum of the Earth's atmosphere. At the excitation wavelength used in this work, the B state is unbound, and immediately dissociates to produce O(^1D) partnered by O(^3P). When a polarized laser is used to carry out the photolysis, the angular distribution of the photofragments relative to the laser polarization axis takes the form[5]

$$P(\theta_v) = 1 + \beta P_2(\cos\theta_v) \quad (3)$$

where θ_v is the angle between the fragment recoil velocity and the laser polarization axis, and $P_2(\cos\theta_v) \propto (1/2)(3\cos^2\theta_v - 1)$ is the second Legendre polynomial. In general, the spatial anisotropy parameter β can take values between –1 and 2. For the B to X transition in O_2, the transition dipole lies parallel to the O−O bond and β takes its limiting value of 2, corresponding to a cosine-squared distribution of the photofragments about the electric vector of the photolysis light. In other words, the O(^1D) and O(^3P) fragments recoil preferentially along the polarization vector of the laser beam.

As noted earlier, observation of Larmor precession relies on the preparation of a strongly aligned distribution of atomic angular momenta. We have shown in previous work[6] that the O($^1D_2$) atoms formed during dissociation of the B state of O_2 are strongly aligned with their electronic angular momentum perpendicular to their recoil velocity. To place this on a more quantitative basis, for an atom with total angular momentum quantum number $J = 2$, the angular momentum distribution arising from photolysis through a pure parallel transition is given by[7]

$$P(\theta_J) = 1 + a_0^{\{2\}} P_2(\cos\theta_J) + a_0^{\{4\}} P_4(\cos\theta_J) \quad (4)$$

where θ_J is the angle between the photofragment angular momentum vector **J** and its recoil velocity **v**, and $P_2(\cos\theta_J)$ and $P_4(\cos\theta_J)$ are second- and fourth-order Legendre polynomials. The parameters $a_0^{\{2\}}$ and $a_0^{\{4\}}$ are alignment parameters, which, in addition to characterizing the angular momentum polarization, may be used to determine the M_J state populations and electron density distribution. These were found to take values of -0.80 ± 0.04 and 0.14 ± 0.02 for $a_0^{\{2\}}$ and $a_0^{\{4\}}$, respectively. Figure 1 presents the distribution of **J** for the nascent O(^1D) as calculated from equation (4), together with the M_J state populations and the corresponding distribution of unpaired electron density. Taking the recoil vector as the quantization axis, ~80% of the O(^1D) atoms are formed in $M_J = M_L = 0$, with a minor contribution from $M_J = 1$, and very little production in $M_J = 2$. This is a highly non-statistical M_J distribution, which corresponds to **J** lying preferentially perpendicular to the recoil velocity, as shown in Fig. 1. Unsurprisingly, the electron density distribution (also shown in Fig. 1) is also highly polarized. Other work[8] has shown that the strong alignment is virtually independent of wavelength as long as the dissociation is dominated by the B state. The alignment persists for dissociation wavelengths all the way from threshold at 175 nm down to ~120 nm, covering the entire range of the Schumann–Runge absorption bands and continuum. Two-photon photolysis, in which the first photon excites to the $b^1\Sigma_g^+$ state and the second to the B state[9], and dissociation via the higher-lying $E^3\Sigma_u^-$ state[10], which shares its short-range repulsive wall with the B state, have also been shown to yield similar alignment in the O(^1D) fragments. Although a fully quantitative quantum theoretical treatment of the dissociation is still a work in progress, the measured M_J distribution approaches that predicted by a diabatic dissociation model[11].

The long lifetime and strongly polarized angular momentum distribution of O($^1D_2$) atoms formed in the UV photolysis of O_2 allows their precessional motion in a magnetic field to be studied over a long timescale. As we shall show, VMI allows direct visualization of the precessional motion. The ease with which an external magnetic field can be used to manipulate the atomic angular momentum distribution (and therefore also the unpaired electron density distribution from which the angular momentum originates) also opens up the intriguing possibility of studying chemical reactions as a function of atomic orbital orientation.

Overview of experiment

The experiments and the VMI spectrometer shown in Fig. 2 are described in detail in the Methods. Here, we provide a brief overview of the experimental technique sufficient to understand the data presented in the Results section.

A molecular beam of O_2 is intercepted by a 157 nm pump laser beam. As described earlier, this excites the O_2 to the B state, from which it dissociates into a ground state O(^3P) atom and an excited state O(^1D) atom. Both atoms have a single well-defined velocity of ~2,200 m s^{-1}, determined by conservation of energy and momentum, such that the atoms recoil from the crossing region on the surface of an expanding spherical shell (or 'Newton sphere'). The O(^1D) photofragments have a $\cos^2\theta$ angular distribution about the polarization vector of the photolysis laser, and their electronic angular momentum vector **J** is strongly aligned perpendicular to their direction of recoil.

The O(^1D) atoms are exposed to a magnetic field generated by a Helmholtz coil, and undergo Larmor precession for a short period of time before being ionized by a second laser pulse and extracted to a position-sensitive detector by an electric field maintained between a set of velocity-mapping electrodes. The detector is time-gated such that each recorded image represents a thin slice through the O(^1D) Newton sphere, corresponding to the detection of products with a fixed value v_z of the recoil velocity component along the time-of-flight (TOF) axis. The laser technique used to ionize the O(^1D) atoms in the probe step is sensitive to the projection of **J** onto the laser polarization axis. As the distribution of atomic angular momentum vectors produced in the photolysis step rotates under the influence of the magnetic field generated by the Helmholtz coils, the detection sensitivity for atoms scattered in different directions changes, allowing the rotation of **J** to be observed clearly in the final images as the applied magnetic field is increased.

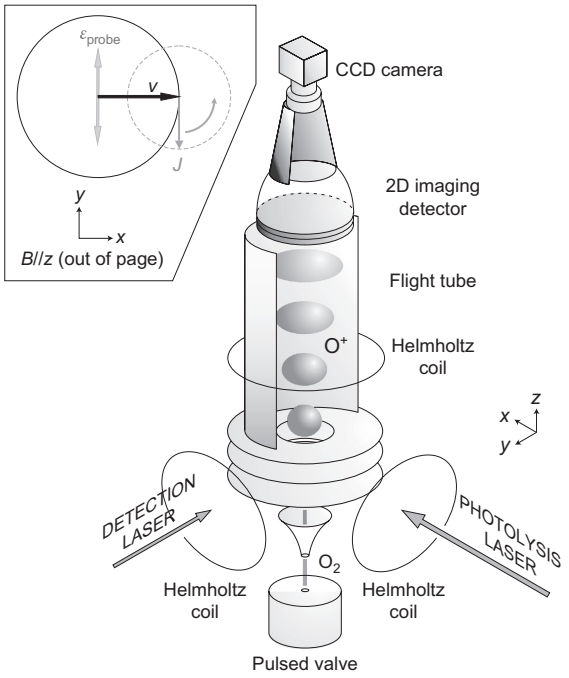

Figure 2 | Schematic of the VMI setup. A molecular beam of O_2 enters the velocity mapping lens along the TOF (z) axis and is crossed in the ionization region by a 157 nm photolysis laser (propagating along the x axis) and a 205.5 nm detection laser (propagating along the y axis). The resulting distribution of O^+ ions is projected onto a 2D position-sensitive detector and the subsequent image recorded by a charge-coupled device camera. Magnetic fields are applied along the x, y, or z axes using Helmholtz coils to initiate precessional motion of the electronic angular momentum vector of the scattered atoms. A schematic diagram of the O(^1D) product angular momentum distribution precessing about a magnetic field **B** applied along the z axis is shown in the inset. ε_{probe} denotes the polarization axis of the probe laser beam.

Several different experimental geometries, defined by the polarization directions of the pump and probe laser beams and the axis along which the magnetic field is applied, have been used to visualize the precessional motion (Supplementary Fig. S1). We describe one representative result in detail here, and present the results measured in this and other geometries in the form of 'Movies' in the Supplementary Information. The geometry to be discussed is shown as an inset to Fig. 3: the photolysis laser is unpolarized, the probe laser is polarized in the image plane and parallel to the photolysis propagation axis, and the magnetic field is applied along the **z** or TOF axis. The pump–probe delay time for this data set is fixed at 80 ns.

Results and discussion

Figure 3 shows a montage of images for O(^1D) precession about a magnetic field applied along the TOF axis. Each triplet of images represents three slices taken through the 3D scattering distribution at three different values of v_z, with the second image in each triplet corresponding to a slice through the centre of the velocity distribution.

The unpolarized 157 nm photolysis laser propagates from top to bottom in the images, so that its electric vector is cylindrically symmetric about the vertical axis of the images. Because the O(^1D) atoms recoil preferentially along the polarization direction, they are also distributed with cylindrical symmetry about the laser propagation axis, with the result that the centre slice recorded in the velocity map image shows intensity to the left and right of the images (perpendicular to the laser propagation axis), and no intensity at the top and bottom (along the laser propagation axis). Application of an external magnetic field may affect the image in two ways. First, the trajectories of the ions as they travel along the flight tube may be perturbed by the presence of the field. This appears to be a very minor effect: as the magnetic field is increased, the velocity-map images are indeed displaced from centre, but not significantly. The second and much more important consideration is the effect of the applied field on the polarized angular momentum distribution of the photofragments. As explained previously, the angular momentum distribution precesses about the field axis at a Larmor frequency determined by the field strength. Because the transition dipole moment for the probe step is correlated with the total angular momentum vector **J**, as the distribution precesses, the detection sensitivity changes, causing the image to undergo apparent rotation with increasing magnetic field strength. We stress that although it may appear from the images that the velocity distribution of the fragments is rotating, this is not the case. The velocity distribution remains unchanged as a function of field strength, but the ionization probability in the probe step for products scattered at different angles changes as the **J** distribution rotates.

The images shown in Fig. 3 are recorded as a function of the current supplied to the Helmholtz coils. The field strength in the interaction region was not measured directly, but can be estimated from the geometry of the Helmholtz coils to range between ~0 and 22 G ($1\ G = 1 \times 10^{-4}$ T) for coil currents of 0–950 mA. At the very lowest field strengths, contributions from the Earth's magnetic field and stray fields from other electronics within the laboratory may perturb the magnetic field experienced by the nascent photofragments, but these effects become negligible at higher field strengths.

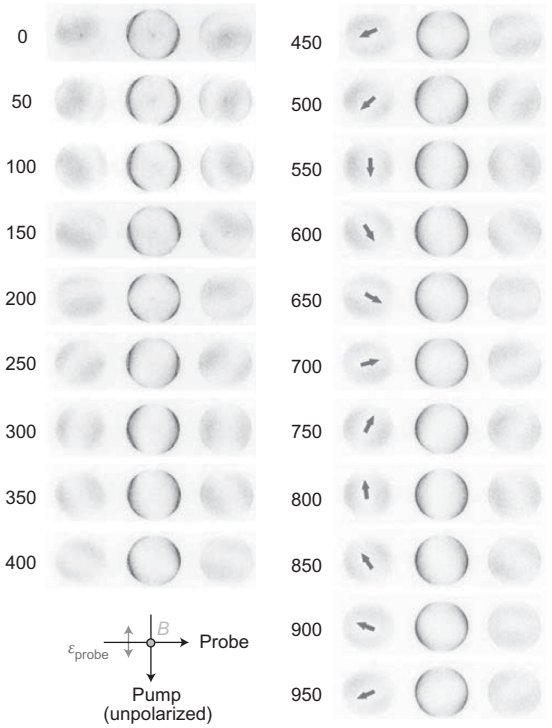

Figure 3 | Montage of 2D sliced images from Supplementary Movie 1. Darker regions correspond to higher signal levels. Three images, taken at early, medium and late arrival times within the O^+ TOF peak are shown from left to right for each value of the current (in mA) applied to the Helmholtz coils. The unpolarized 157 nm dissociation laser (propagating along the x axis in Fig 2) crosses perpendicular to the 205.5 nm probe laser (y axis), which is polarized in the x direction (the polarization axis is denoted by ε_{probe}). Arrows are included to guide the eye in the direction of rotation of the angular momentum polarization.

Figure 4 | Experimentally measured and simulated images for the subset of images from Fig. 3 spanning Helmholtz coil currents of 200–450 mA. The magnetic field strengths used in the simulations are shown to the right of the images. Details of the simulations are given in the text.

Using equation (2), we can calculate the Larmor precession frequency ν_L (in units of s^{-1}) to be

$$\nu_L = \frac{\mu_B B}{h} = 1.3996 \times 10^{10} B \qquad (2)$$

where the field strength B is given in tesla. We can therefore predict that to achieve a full rotation of the angular momentum distribution the magnetic field strength must be scanned over a range of ~9 G at the 80 ns pump–probe delay time used in the present measurements. The Earth's magnetic field is 0.3–0.6 G, so without an applied field the precessional period is ~1 μs. As indicated in the images shown in Fig. 3, a full rotation occurs between coil currents of 450 and 950 mA, corresponding to an approximate change in field strength B of ~11 G based on our estimate of the magnetic field at a given coil current. For a given set of alignment parameters, it is fairly straightforward to simulate the images that would be expected for particular values of the applied magnetic field, and we have carried out Monte Carlo simulations to model our experimental images. In addition to demonstrating a full understanding of the physical processes occurring in our experiment, the simulations also allow a more rigorous calibration of the magnetic field than is possible in the simple calculations outlined above.

To simulate the centre slice of the measured distribution, for each ion trajectory we first randomly sample a velocity in the image plane from the O(^1D) velocity distribution, $P(\theta_v) \propto 1 + \beta P_2(\cos\theta_v)$ (eq. (3)). We can then determine the image coordinates ($x = v\cos\theta_v$, $y = v\sin\theta_v$), where v is the speed of the O(^1D) fragment. Because we are only interested in the angular dependence of the images, v was set to 1 for the simulations. Next, we select polar angles θ_J and ϕ_J for **J** relative to **v**, and determine the probability of the fragment having this polarization from equation (4). During the pump–probe delay time τ, the applied magnetic field causes the angular momentum **J** to precess through an angle $\phi_B = 2\pi\nu_L\tau$, where ν_L is the Larmor frequency defined in equation (2).

To determine the detection probability for the ion, it is necessary to determine the projection of the transition dipole $\boldsymbol{\mu}_{probe}$ for the resonance-enhanced multiphoton ionization (REMPI) step onto the (laboratory frame) probe laser polarization. For the probe transition used, $\boldsymbol{\mu}_{probe}$ is perpendicular to **J**, and the appropriate projection may be determined from the polarization of **J** in the laboratory frame. Determining **J** in the laboratory frame (that is, relative to the photolysis laser polarization), rather than in the molecular frame in which it is currently defined (that is, relative to **v**) simply involves rotating **J** first through the angle θ_v between **v** and the photolysis polarization vector, and then through the precession angle ϕ_B. In this manner we determine the appropriate projection onto the probe laser polarization vector, and convert this to a detection probability.

Figure 4 shows a comparison between the results of these simulations and the experiments for the geometry shown in Fig. 3. The agreement between the experimental and simulated data is good, with small discrepancies probably arising due to residual or stray fields in the experiment that have not been characterized, and that cannot therefore be modelled in the simulations. The dependence of the magnetic field on the Helmholtz coil current, determined by comparing the experimental and simulated images, is shown in Fig. 5.

Our observations of Larmor precession in O($^1D_2$) atoms demonstrate that the laboratory-frame orientation of an aligned or oriented angular momentum distribution is readily controlled by the application of a relatively weak magnetic field. There are numerous consequences that are worth exploring, one of which is the effect of precessional motion on atomic emission of radiation. When an excited state molecule emits a photon to return to the ground state, the photon polarization is correlated with the transition dipole moment for the emission, so that an aligned or oriented distribution of excited state molecules emits polarized radiation. Fluorescence from an aligned or oriented angular momentum distribution rotating under the influence of a magnetic field therefore displays a sinusoidal oscillation in intensity when viewed through a polarizer. This effect is well known, and techniques such as quantum-beat spectroscopy take advantage of the phenomenon to characterize aligned or oriented distributions of excited state molecules[12,13]. As well as allowing such fundamental studies, the effect of a magnetic field on the properties of polarized radiation is potentially of considerable interest in relation to processes occurring in the interplanetary medium, interstellar medium, circumstellar regions and quasars. Our experiments generate highly polarized distributions of O(^1D) atoms in a photolysis process that also occurs widely in the Earth's atmosphere, and it is worth considering at this point whether our findings have any consequences for atmospheric chemistry.

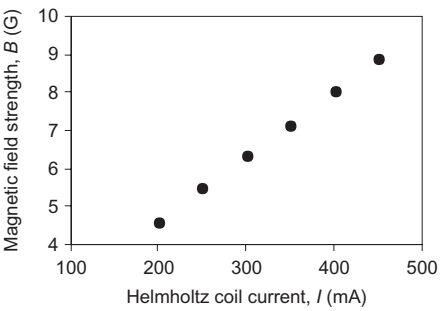

Figure 5 | Calibration showing the dependence of the magnetic field strength experienced by the scattered O($^1D_2$) atoms on Helmholtz coil current. The curve was derived by comparing computer simulations of the photofragment velocity-map images at various field strengths with the experimentally measured images.

The maximum solar energy absorption of O_2 in the Schumann–Runge continuum through the process

$$O_2 + h\nu(\lambda \leq 175\ \text{nm}) \rightarrow O(^1D) + O(^3P)$$

occurs in the Earth's mesosphere and lower thermosphere at altitudes of 80–110 km. This corresponds well with the region in which the $O(^1D)$ daytime emission (dayglow) reaches a maximum[2]. At the lower altitudes of 10–50 km spanned by the Earth's stratosphere, $O(^1D)$ is produced by photodissociation of ozone in the Hartley bands through the process

$$O_3(X^1A_1) + h\nu(200-320\ \text{nm}) \rightarrow O(^1D) + O_2(^1\Delta_g)$$

This process is also known[14] to lead to the production of highly polarized $O(^1D)$ atoms over the wavelength range 235–305 nm, again with M_J state populations peaking at $M_J = 0$.

Applying a simple model in which the incident sunlight is polarized in a plane perpendicular to the Earth–Sun axis along which it propagates (note that this assumes no scattering and depolarization of light by other atmospheric constituents before absorption), there would appear to be plenty of scope for the production of $O(^1D)$ atoms with angular momenta that are aligned with respect to the direction of the incoming sunlight. This raises the question of whether such polarization is amenable to observation, for example, through polarization of the dayglow emission. The answer to this question lies in a consideration of the various competing processes for removal and/or depolarization of $O(^1D)$. $O(^1D)$ atoms are both depolarized and quenched to the $O(^3P)$ electronic ground state in collisions with N_2 and O_2, which occur on a timescale much faster than the $O(^1D)$ radiative lifetime[15]. The collisional quenching cross-section for $O(^1D) \rightarrow O(^3P)$ is large, of the order of 4×10^{-11} cm^3 s^{-1}. However, it is clear that not every collision leads to electronic quenching, as it has been shown that $O(^1D)$ is translationally thermalized under atmospheric conditions. If these thermalizing collisions also cause depolarization, then this accounts for the fact that polarized dayglow emission has not been observed. Even in the absence of collisions, Larmor precession of the nascent polarized angular momentum of the $O(^1D)$ in the Earth's magnetic field would essentially randomize the polarization for long-lived $O(^1D)$ atoms emitting over a broad range of times. In lower density environments, such as the interstellar medium, where the time between collisions greatly exceeds the radiative lifetime, atomic polarization almost certainly survives for long enough to be observable in emission, and may be a potential probe of local magnetic fields.

Of more interest to terrestrial activities, the long lifetime and strong polarization of $O(^1D)$ formed in the UV photolysis of O_2 or O_3 makes it an extremely promising candidate for laboratory-based studies into the effects of atomic polarization on bimolecular collisions, and on chemical reactivity more generally. Such effects were first observed by Rettner and Zare[3], who found that the alignment axis in laser-pumped $Ca(^1P)$ atoms strongly affects the branching ratio between different CaCl* electronically excited products states formed following reaction with HCl. Orbital alignment effects have since been studied for a variety of bimolecular processes[4,16]. Reactions of $O(^1D)$ with methane, for example, have been investigated in great detail[17]. The $O(^1D)$ reactant for these bimolecular reaction studies was generated through O_2 photodissociation at 157 nm (ref. 18), and therefore had the same angular momentum distribution as shown in Fig. 1. Our work opens up the possibility of measuring the reactivity and product state distributions for this and other chemical systems while using a magnetic field to control the direction of the $O(^1D)$ electron density and angular momentum with respect to the collision partner.

Methods

The VMI apparatus has been described in detail in Ref. 4, and is shown schematically in Fig. 2. In brief, a pulsed supersonic expansion of O_2 at a stagnation pressure of 1 bar was skimmed before entering the electrostatic lens assembly used to achieve velocity-mapping conditions. Half way between the first two lens elements, the molecular beam was crossed by the photolysis laser (157 nm) and probe laser (205.5 nm), which were arranged to cross at right angles. For the measurements reported here, the photolysis laser beam was unpolarized, and the probe laser was polarized either parallel or perpendicular to the image plane using a variable waveplate. Detection of the $O(^1D_2)$ photolysis products was through the $^1D_2 \rightarrow 3p^1P_1$ (2 + 1) REMPI transition.

Three Helmholtz coils centred on the $\boldsymbol{x}$, $\boldsymbol{y}$ and $\boldsymbol{z}$ axes defined in Fig. 2 (with $\boldsymbol{z}$ lying along the TOF direction and $\boldsymbol{x}$ and $\boldsymbol{y}$ coinciding with the laser propagation directions) were used to provide the magnetic fields required to initiate precessional motion of the photofragment angular momentum. Photodissociation of O_2 at 157 nm yielded $O(^1D)$ atoms with a velocity of ~2,200 m s^{-1} and strongly aligned electronic angular momentum, as outlined in the previous section. Atoms with the same alignment distribution could in principle be created at any velocity up to ~6,000 m s^{-1} by dissociation of O_2 at other wavelengths within the Schumann–Runge continuum, which ranges from 175 to 120 nm. During the pump–probe delay time, the angular momentum distribution precesses about the magnetic field applied using the Helmholtz coils, before the fragments are ionized by means of (2 + 1)REMPI and detected. Precession of **J** may in principle be imaged either by fixing the magnetic field strength **B** and recording images for increasing pump–probe delay times, or by fixing the delay and recording images as a function of **B**. In this work the images were recorded using an optical slice-imaging technique (described in detail in ref. 4), and under these conditions timing considerations make it much more straightforward to fix the pump–probe delay and vary the magnetic field strength. Consequently, images were recorded as a function of **B** for two different laser pump–probe delay times τ of 80 and 400 ns. The precessing atoms travelled less than 1 mm in the time between their formation and ionization, even for the longer of the two pump–probe delay times, and it is assumed that the applied magnetic field was sufficiently spatially homogeneous over this distance scale that inhomogeneity effects did not need to be considered. This assumption is supported by the results of the simulations presented in the Results.

The Supplementary movies were generated from sequences of images recorded as a function of increasing magnetic field strength. In the main text we discuss the data corresponding to the experimental geometry shown in the inset to Fig. 3 at a pump–probe delay of 80 ns (Supplementary Movie 1). Other geometries that were used are listed in Supplementary Fig. S1.

Received 4 August 2010; accepted 5 November 2010; published online 12 December 2010

References

1. Bernath, P. F. *Spectra of Atoms and Molecules* (Oxford Univ. Press, 1995).
2. Wayne, R. P. *Chemistry of Atmospheres* 2nd edn (Oxford Univ. Press, 1990).
3. Rettner, C. T. & Zare, R. N. Effect of atomic reagent approach geometry on reactivity—reactions of aligned $Ca(^1P_1)$ with HCl, Cl_2 and CCl_4. *J. Chem. Phys.* **77,** 2416–2429 (1982).
4. Janssen, M. H. M., Parker, D. H. & Stolte, S. Steric effects on electronically excited product channels in reactions between $Ca(^1D_2)$ and CH_3X(JKM) (X = Cl, Br). *J. Phys. Chem.* **100,** 16066–16071 (1996).
5. Zare, R. N. *Angular Momentum: Understanding Spatial Aspects in Chemistry and Physics* (John Wiley & Sons, 1988).
6. Wu, S.-M. *et al.* Angular momentum polarisation in the $O(^1D)$ products of O_2 photolysis via the $B(^3\Sigma_u^-)$ state. *Mol. Phys.* **108,** 1145–1157 (2010).
7. Rakitzis, T. P. & Zare, R. N. Photofragment angular momentum distributions in the molecular frame: determination and interpretation. *J. Chem. Phys.* **110,** 3341–3350 (1999).
8. Parker, D. H. Laser photochemistry of molecular oxygen. *Acc. Chem. Res.* **33,** 563–571 (2000).
9. Eppink, A. T. J. B., Parker, D. H., Jansenn, M. H. M., Buijsse, B. & van der Zande, W. J. Production of maximally aligned $O(^1D)$ atoms from two-step photodissociation of molecular oxygen. *J. Chem. Phys.* **108,** 1305–1308 (1998).
10. Lambert, H. M., Dixit, A. A., Davis, E. W. & Houston, P. L. Quantum yields for product formation in the 120–130 nm photodissociation of O_2, *J. Chem. Phys.* **121,** 10437–10446 (2004).
11. Singer, S. J., Freed, K. F. & Band, Y. B. Theory of diatomic molecule photodissociation—electronic angular momentum influence on fragment and fluorescence cross-sections. *J. Chem. Phys.* **79,** 6060–6085 (1983).
12. Treffers, M. A. & Korving, J. Precession induced modulation of fluorescence. *J. Chem. Phys.* **85,** 5076–5084 (1986).
13. Yan, H. & Lazarian, A. Optical polarization from aligned atoms as a new diagnostic of astrophysical magnetic fields. In *Conference Series, Astronomical Polarimetry: Current Status and Future Directions* (eds Adamson, A., Aspin, C. & Davis, C.) Vol. 343, 346–351 (Astronomical Society of the Pacific, 2005).
14. Dylewski, S. M., Geiser, J. D. & Houston, P. L. The energy distribution, angular distribution, and alignment of the $O(^1D_2)$ fragment from the photodissociation of ozone between 235 and 305 nm. *J. Chem. Phys.* **115,** 7460–7473 (2001).

15. Chowdhury, A. M. S. Studies on the competing collisional relaxation dynamics of superthermal $O(^1D)$ atoms in the upper atmosphere by ultraviolet laser spectroscopy. *Laser Phys.* **9,** 959–989 (1999).
16. Zare, R. N. Laser control of chemical reactions. *Science* **279,** 1875–1879 (1998).
17. Brouard, M., Lambert, H. M., Short, J. & Simons, J. P. Product state-resolved stereodynamics of the reaction $O(^1D) + CH_4 \rightarrow OH + CH_3$. *J. Phys. Chem.* **99,** 13571–13581 (1995).
18. Lin, J. J., Shu, J., Lee, Y. T. & Yang, X. Multiple dynamical pathways in the $O(^1D) + CH_4$ reaction: a comprehensive crossed beam study. *J. Chem. Phys.* **113,** 5287–5301 (2000).

Acknowledgements

The authors acknowledge support from the European Union under training network ITN 238671 'ICONIC', the European Research Council under Starting Independent Research Grant 200733 'ImageMS', the Dutch National Science Foundation FOM-NWO program Molecular Atmospheric Processes, and the National Science Foundation under NSF CHE 0650414.

Author contributions

D.P., W.Z. and, independently, R.Z., conceived and designed the experiments. S.W. and D.R. performed the experiments. C.V. and G.G. analysed the data. C.V., D.P. and S.W. wrote the manuscript, with contributions from W.Z., G.G. and R.Z.

Additional information

The authors declare no competing financial interests. Supplementary information accompanies this paper at www.nature.com/naturechemistry. Reprints and permission information is available online at http://npg.nature.com/reprintsandpermissions/. Correspondence and requests for materials should be addressed to D.P., C.V. and R.Z.